NASA TECHNICAL MEMORANDUM

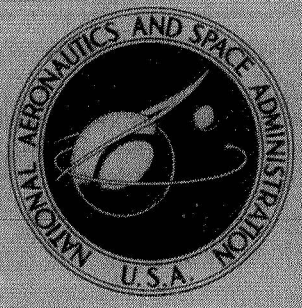

NASA TM X-1947

NASA TM X-1947

PERFORMANCE AND STALL LIMITS OF AN AFTERBURNER-EQUIPPED TURBOFAN ENGINE WITH AND WITHOUT INLET FLOW DISTORTION

by Roger A. Werner, Mahmood Abdelwahab, and Willis M. Braithwaite

Lewis Research Center
Cleveland, Ohio

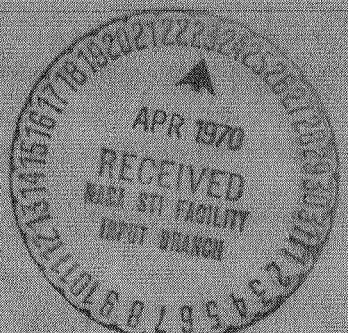

NATIONAL AERONAUTICS AND SPACE ADMINISTRATION • WASHINGTON, D. C. • APRIL 1970

1. Report No. NASA TM X-1947	2. Government Accession No.	3. Recipient's Catalog No.
4. Title and Subtitle PERFORMANCE AND STALL LIMITS OF AN AFTERBURNER-EQUIPPED TURBOFAN ENGINE WITH AND WITHOUT INLET FLOW DISTORTION		5. Report Date April 1970 6. Performing Organization Code
7. Author(s) Roger A. Werner, Mahmood Abdelwahab, and Willis M. Braithwaite		8. Performing Organization Report No. E-5352
9. Performing Organization Name and Address Lewis Research Center National Aeronautics and Space Administration Cleveland, Ohio 44135		10. Work Unit No. 720-03 11. Contract or Grant No.
12. Sponsoring Agency Name and Address National Aeronautics and Space Adminstration Washington, D. C. 20546		13. Type of Report and Period Covered Technical Memorandum 14. Sponsoring Agency Code
15. Supplementary Notes		

16. Abstract

Performance and stall limits of a nonstandard TF30-P-1 turbofan engine with uniform and distorted inlet flow are presented at a Reynolds number index of 0.5. Screens covering a 180° sector of the inlet were used to obtain the distortion. Results are presented in the form of compressor performance maps, stall limits, bypass ratio, stage-group characteristics, distortion levels, and inlet profiles.

17. Key Words (Suggested by Author(s))	18. Distribution Statement
Turbofan Compressor stall Inlet flow distortion Screens	Unclassified - unlimited

19. Security Classif. (of this report)	20. Security Classif. (of this page)	21. No. of Pages	22. Price *
Unclassified	Unclassified	34	$3.00

*For sale by the Clearinghouse for Federal Scientific and Technical Information Springfield, Virginia 22151

PERFORMANCE AND STALL LIMITS OF AN AFTERBURNER-EQUIPPED TURBOFAN ENGINE WITH AND WITHOUT INLET FLOW DISTORTION

by Roger A. Werner, Mahmood Abdelwahab, and Willis M. Braithwaite

Lewis Research Center

SUMMARY

An investigation was conducted to determine the performance and stall limits of a nonstandard TF30-P-1 turbofan engine with uniform inlet flow and 180° circumferential screen distorted inlet flow. The turbofan is a two-spool engine equipped with an afterburner and is typical of those consider for supersonic aircraft. Performance maps showing the effect of exhaust nozzle variation are presented for the fan hub and tip regions, the low-pressure compressor, and the high-pressure compressor. Stall limits are indicated on each of the four performance maps. Steady-state data are also presented as pressure and flow coefficients for stage groups of three to four stages. The effects of inlet flow distortion produced by four screen solidities on steady-state performance, stall lines, and stage-group characteristics are presented. Typical inlet flow distortion patterns are also shown. Inlet conditions were simulated for a Reynolds number index of 0.5.

Stall-limited inlet pressure distortions ranged to a maximum K_{D2} of 1100 (6 percent $\Delta P_t/P_{t,av}$) at a corrected airflow of 240 pounds per second (109 kg/sec). The distorted inlet flow reduces the performance of the fan and low-pressure compressor along the rated operating lines and lowers the stall lines. The stall lines of the low-pressure compressor intersect the rated nozzle area operating line at progressively lower speeds as the distortion increases. The high-pressure compressor appears to be unaffected by the inlet flow distortions.

INTRODUCTION

A major problem encountered in the development of new high-performance supersonic aircraft has been the achieving of propulsion system stability. This problem re-

sulted from distortions of the flow field at the discharge of the supersonic inlet and an inadequate understanding of the effects of such flow fields on engine stability.

An experimental program is being conducted to study the effects of flow fields on engine stability. A two-spool turbofan engine, typical of those being used or planned for supersonic aircraft, was selected for this program. A high-response pressure measurement capability (ref. 1) was used to determine the origin and progression of stall through the compressor.

Steady-state inlet flow distortions have been simulated at the engine inlet by use of screens (refs. 2 to 5). This report is concerned with the effects of this type of inlet flow distortion on engine performance and stall limits. Four simple 180° circumferential patterns were selected for this program.

Data are presented for a Reynolds number index of 0.5 over a range of corrected inlet airflows and exhaust nozzle areas. The results are presented in the form of compressor performance maps, stall limits, stage-group characteristics, distortion levels, and inlet profiles.

APPARATUS

The engine, instrumentation, and inlet airflow distortion screens are discussed in this section. A brief description is also given of the engine installation in the facility.

Engine

The engine used for this investigation was a Pratt & Whitney nonstandard TF30-P-1 two-spool turbofan. The compressors and combustor section were standard production P-1 items while the turbine and afterburner-tailpipe were of a preproduction configuration. The preproduction turbine would cause the low-pressure compressor to have a slightly higher operating line (approx. 2 percent). Therefore, the data obtained with this engine would indicate valid trends, but not necessarily representative levels, of performance typical of production P-1 engines.

The physical layout of the engine, shown schematically in figure 1, consists of a three-stage axial-flow fan mounted on the same shaft with a six-stage axial-flow low-pressure compressor. This unit is driven by a three-stage low-pressure turbine. A seven-stage axial-flow high-pressure compressor is driven by a single-stage air-cooled turbine. The nominal overall pressure ratio of the compressor system is 17:1 with a

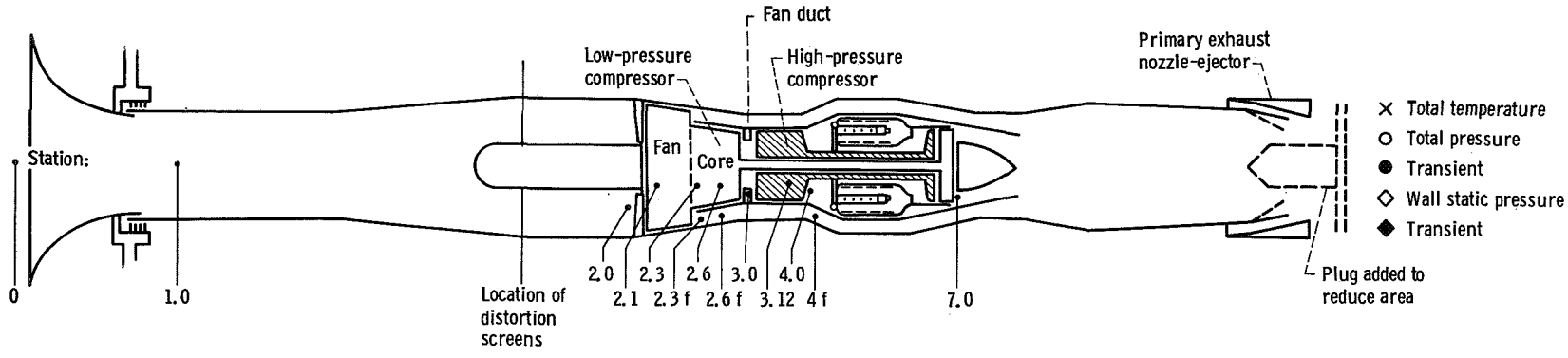

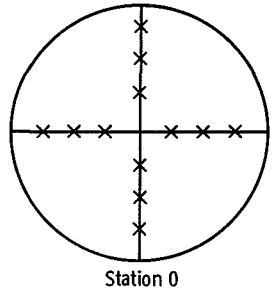

Station 0

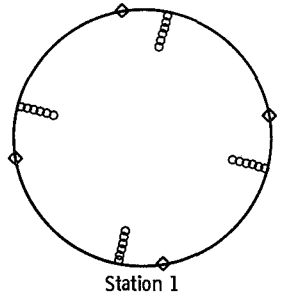

Station 1

(Airflow metering station))

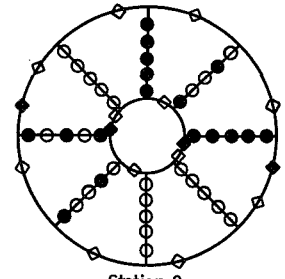

Station 2

(Fan inlet)

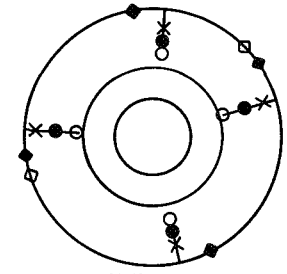

Station 2.1

(In first-stage stator passage)

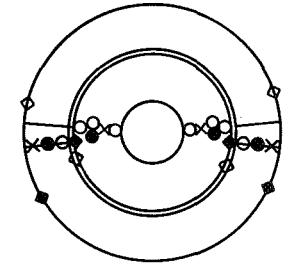

Stations 2.3 and 2.3 f

(Fan discharge and low-pressure compressor inlet)

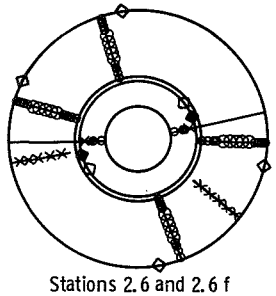

Stations 2.6 and 2.6 f

(In sixth-stage stator passage and fan duct)

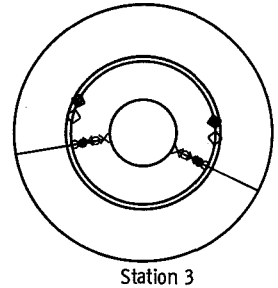

Station 3

(Low-pressure compressor discharge; high-pressure compressor inlet)

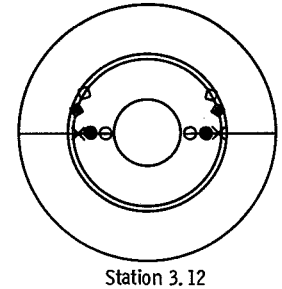

Station 3.12

(In twelfth-stage stator passage)

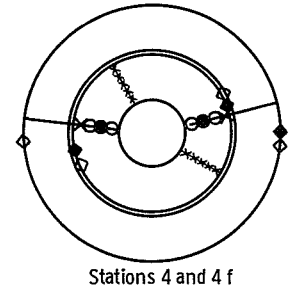

Stations 4 and 4 f

(High-pressure compressor discharge and fan duct)

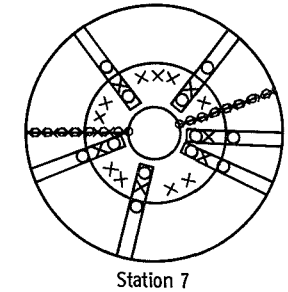

Station 7

(Turbine discharge)

CD-10308-14

Figure 1. - Instrumentation layout for two-spool turbofan engine.

fan bypass ratio of 1. The fan duct airflow is diverted from the core flow by a splitter ring at the exit of the third-stage rotor. It then passes through an annular passage surrounding the core engine and is combined with the turbine discharge gases at the afterburner inlet. The total flow is then discharged through a variable-area exhaust nozzle. An ejector nozzle, having aerodynamically operated blow-in doors and exit leaves, is a part of the normal engine-afterburner assembly. The ejector controls the expansion of the primary jet and pumps cooling and purging air for the engine compartment.

The engine was also equipped with automatic 12th-stage bleeds (third stage of high-pressure compressor). These bleeds open at low engine speeds to aid in acceleration and close when the pressure rise across the low compressor reaches a predetermined value.

Engine modifications. - Several modifications were made to this engine. The afterburner fuel system was deactivated and the afterburner portion of the control was modified such that the primary exhaust nozzle area could be independently increased from full closed to full open (rated area to 193 percent of rated). A plug, not supported by the engine, could be inserted into the nozzle to reduce the area to 72 percent of rated. The blow-in doors and exit leaves were removed from the ejector.

The 12th-stage bleeds were also modified such that they could be placed on automatic operation or could be maintained either in the open or closed position as desired. This permitted obtaining data with the bleeds closed at low speeds and open at high speeds, which would not be possible in the automatic configuration.

Another modification was the incorporation of a fuel-step device. An accumulator, filled with fuel during normal operation, was discharged rapidly by pressurizing it with high-pressure gaseous nitrogen. The fuel was injected into the fuel system between the fuel control and the engine. The size of the step could be controlled by the nitrogen pressure and the length of time that it was supplied to the accumulator.

The 16th-stage (high-pressure compressor exit) bleeds were modified by attaching ducts to the bleed ports. These ducts were connected through two remote-controlled throttling valves, one to the facility exhaust system and the other to the facility high-pressure air system. It was possible to bleed air from the compressor discharge and thus lower the pressure ratio across the compressor or to bleed in high-pressure air and raise the pressure ratio. The inflow bleed system had sufficient capacity to raise the pressure ratio to the stall limit from idle to near rated speeds.

Engine protection systems. - The danger of damage to the engine resulting from exceeding the turbine inlet temperature or rotor speed limits was minimized by modifying the engine control which schedules fuel flow as a function of burner pressure. A three-way valve, inserted in the burner pressure sensing line to the control, was actuated whenever either of these limits was exceeded. This action vented the control to test

chamber pressure (approx. one-sixteenth of atmospheric pressure). The control then reduced the fuel flow to a minimum value. The engine is normally equipped with an automatic relight switch which activates the ignition circuit if the primary combustor blows out. It detects a rapid decrease in burner pressure. This circuit was also modified such that the switch activated the three-way valve instead of the igniters. Thus, the fuel flow was reduced to the minimum when compressor stall caused an abrupt drop in pressure at the compressor discharge. Visual and audible alarms were also triggered by each of these detectors.

Instrumentation

The instrumentation is basically the same as that used in a preceding TF30-P-1 investigation (ref. 1). The station identification and probe locations are shown in figure 1. The stations were selected to divide the compressor into groups of three or four stages. At each station the instrumentation was located in the left and right sides of the engine, providing the capability for evaluating the compressor performance for both the distorted and undistorted flow sectors.

Steady-state instrumentation. - Pressures were recorded on a digital, automatic, multiple-pressure recorder having three pressure ranges: (1) zero to 14 psia ±0.014 psi (9.6 N/cm^2 abs ±0.0096 N/cm^2), (2) zero to 35 psia ±0.035 psi (24 N/cm^2 abs ±0.024 N/cm^2), and (3) zero to 140 psia ±0.14 psi (96 N/cm^2 abs ±0.096 N/cm^2). Shielded Chromel-Alumel thermocouples were used to measure all temperatures, which were recorded on an automatic voltage digitizer. These systems are described in more detail in reference 6.

High-response transient instrumentation. - During an engine stall, the peak pressure duration within the fan and compressor units is less than 10 milliseconds. High-response transient instrumentation and recording systems were used to measure this pressure rise and trace the stall progression through the engine. The number of transient probes and their location are shown in figure 1. This instrumentation was designed to have a frequency response to approximately 300 hertz with a maximum of ±5 percent error in amplitude. The use of small transducers capable of being located within $1\frac{1}{2}$ inches (3.8 cm) from the sense point was required. Thus, most of the transducers were within the engine envelope and subject to a hostile temperature environment. The design, cooling, and methods of calibration and recording of these transducers are discussed in appendix C. Adjacent to each transient pickup, a steady-state pressure measurement was made to provide the calibration base value for the transient data.

Distortion Device

Variation in inlet total pressure distortion was obtained by inserting various mesh screens in the inlet duct. This method has been used by many investigators to simulate steady-state distortions. A typical screen with its supporting structure is shown in figure 2. The screens were positioned 1 duct diameter upstream of the engine. The supporting structure is made up of twelve 0.20- by 1.55-inch (5.08- by 39.37-mm) equally spaced struts and a 0.5 mesh backup screen of 0.120-inch (0.3048-mm) diameter wire.

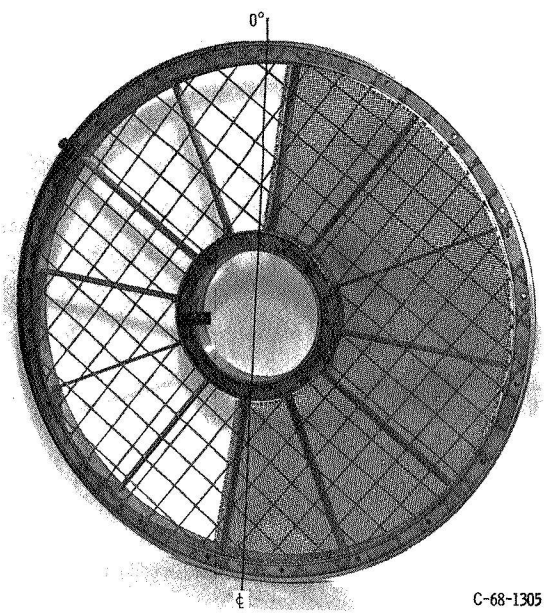

Figure 2. - A typical 180° distortion screen, looking downstream.

The total blockage of the supporting struts and the backup screen is 14 percent. The distortion screens used for this investigation were all of 180° circumferential extent. The four screen configurations are described in the following table:

Screen configuration	Solidity, percent blockage	Mesh	Wire diameter	
			in.	mm
A	35	$5\frac{1}{2}$	0.035	0.889
B	40	$6\frac{1}{2}$	↓	↓
C	20/40	$3/6\frac{1}{2}$		
D	35/40	$5\frac{1}{2}/6\frac{1}{2}$		

In configurations C and D, the 20 and 35 percent solidity screens were laid over the 40 percent screen. Care was taken in alining the two grids at 45^{o} so that the maximum solidity resulted and would be repeatable.

Engine Installation

The engine was installed in an altitude test chamber as shown in figure 3. The installation was a conventional direct-connect type. The altitude chamber includes a for-

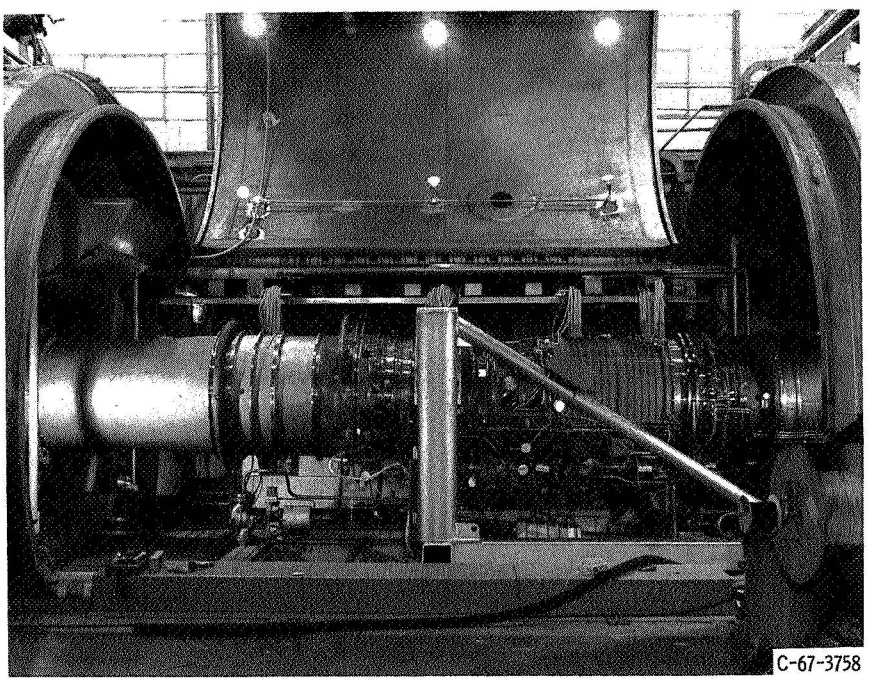

Figure 3. - Turbofan engine installed in altitude test chamber.

ward bulkhead separating the inlet plenum from the test chamber. Conditioned air was supplied to the plenum at the desired pressure and temperature. The conditioned air flowed from the plenum through a bellmouth and duct to the compressor inlet. It was in this duct that the distortion screens were placed. A valve in the bulkhead allowed some of the air to bypass the engine. This valve was automatically controlled to maintain a constant inlet pressure and ram-pressure ratio across the engine during steady-state and normal engine transient operation. The exhaust from the engine was captured by a collector, extending through a rear bulkhead, which minimized the recirculation of exhaust gases into the test chamber. The chamber pressure (altitude pressure) was controlled by an automatic valve.

PROCEDURE

Test Condition

This investigation was conducted at an engine inlet Reynolds number index of 0.5. The inlet total temperature was maintained at approximately 60° F (16° C) and the inlet total pressure adjusted to maintain the Reynolds number index. During operation with distortion, the total pressure in the high-pressure area of the compressor face (which would be related to the flight condition) was held at the desired value by varying the plenum pressure as required.

The ram-pressure ratio across the engine was maintained greater than 3:1 to assure a choked exhaust nozzle at all operating conditions. For this investigation, the exhaust nozzle area was varied from 72 to 193 percent of the rated area. The interstage bleeds were closed except where noted.

Operational Procedure

The stall limits with a given screen were obtained by slowly accelerating the engine from idle speed with the 12th-stage bleeds closed until stall occurred. The fan speed at the occurrence of stall was noted. The engine was subsequently operated at that fan speed with the 12th-stage bleeds open (without the occurrence of stall), and steady-state data obtained. This permitted evaluation with steady-state instrumentation of the inlet distortion that caused a bleeds-closed engine stall. Stall data for inlet distorted flow were also obtained by fuel steps.

The uniform inlet flow engine stalls were initiated by slow accelerations, fuel steps, and 16th-stage inflow bleed.

RESULTS AND DISCUSSION

Uniform Inlet Flow

The measured fan and compressor performance of the turbofan engine are presented on four performance maps. Figures 4 and 5 describe the outer and inner annulus performance of the fan (the first three stages) since each is a different function of the engine exhaust nozzle area. Figure 6 gives the performance of the low-pressure compressor (stages 4 to 9) which is on the same shaft as the fan. The fourth performance map (fig. 7) is for the high-pressure compressor (stages 10 to 16), which is on a second

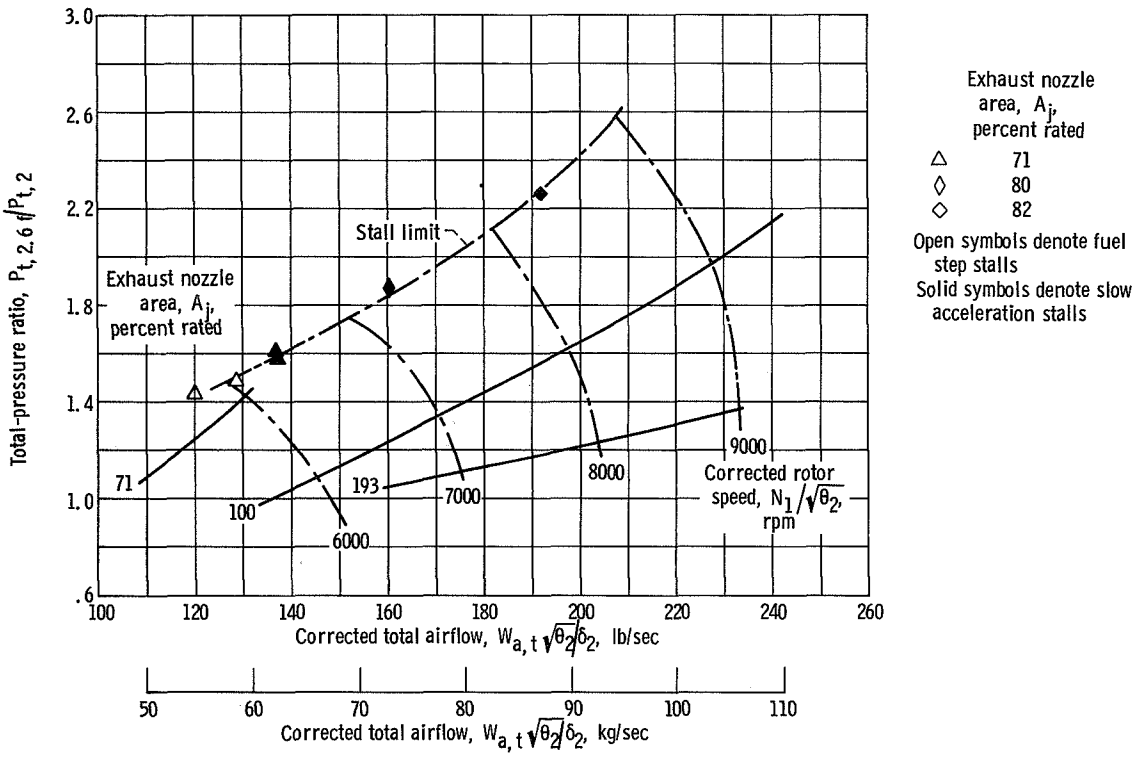

Figure 4. - Fan outer annulus performance at engine inlet Reynolds number index of 0.5, no inlet flow distortion.

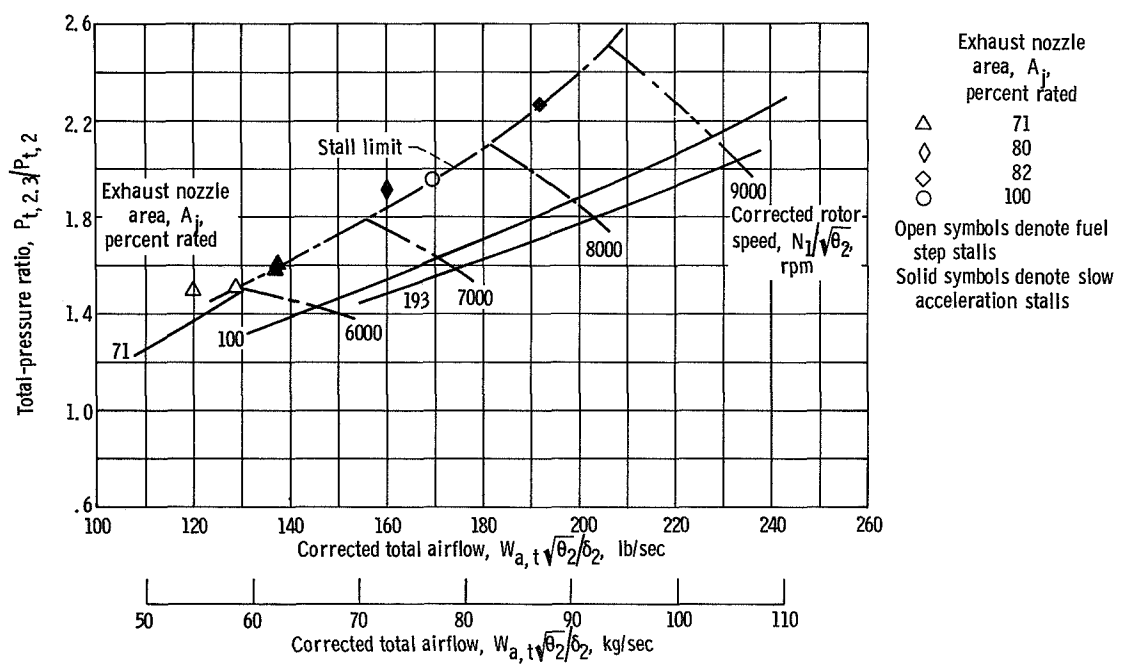

Figure 5. - Fan inner annulus performance at engine inlet Reynolds number index of 0.5, no inlet flow distortion.

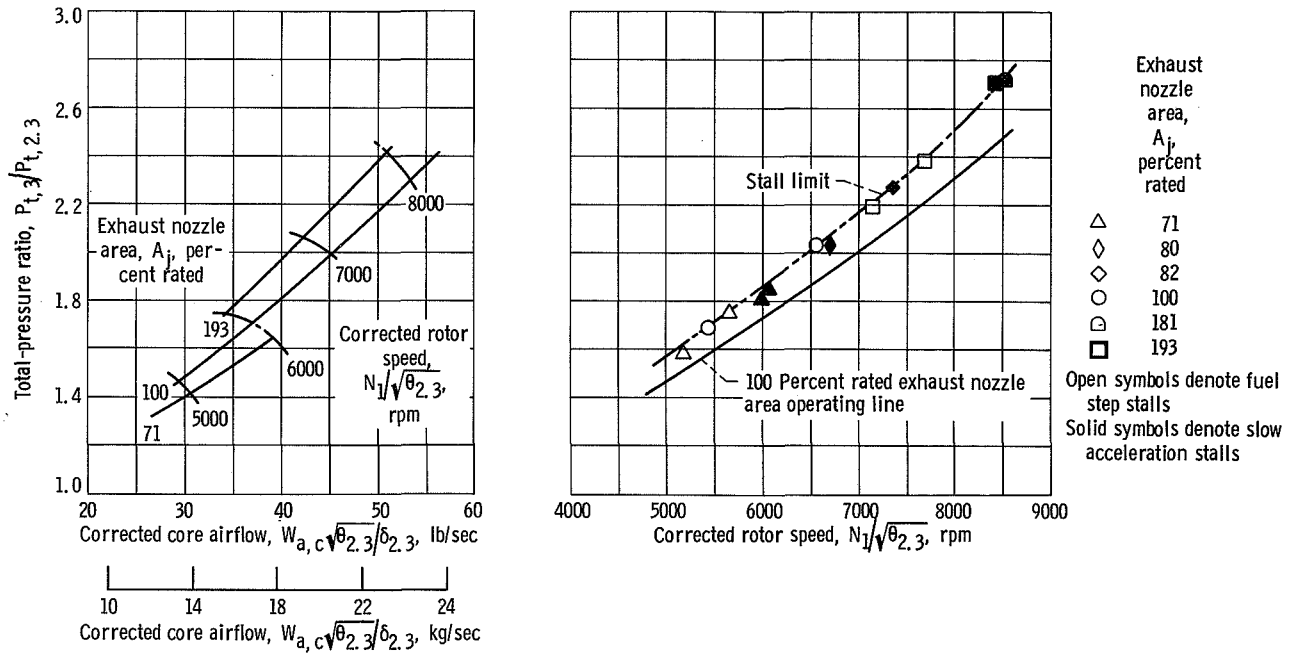

(a) Steady-state performance.

(b) Stall performance.

Figure 6. - Low-pressure compressor performance at engine inlet Reynolds number index of 0.5, no inlet flow distortion.

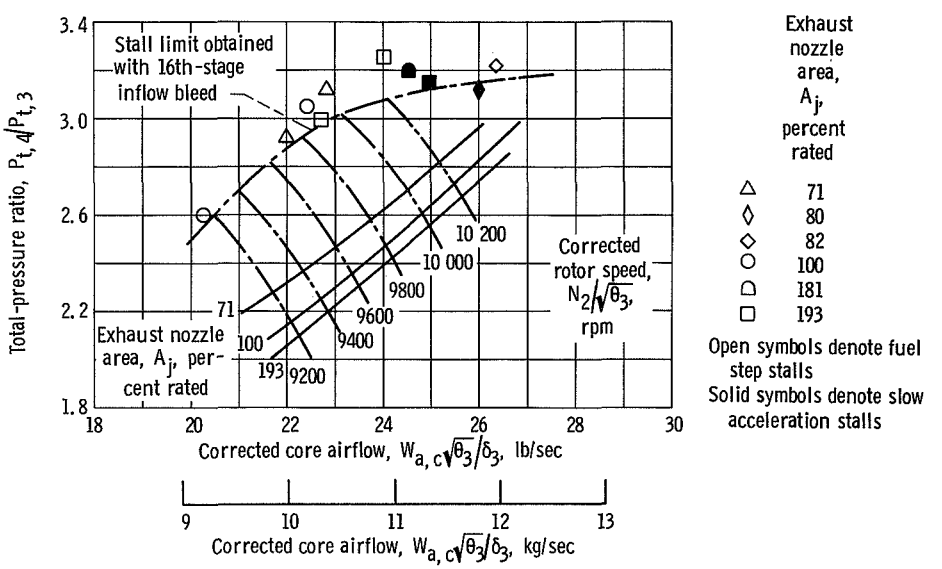

Figure 7. - High-pressure compressor performance at engine inlet Reynolds number index of 0.5, no inlet flow distortion.

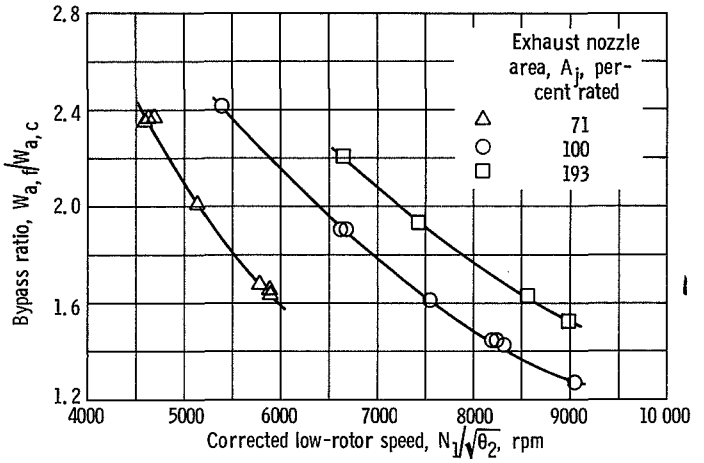

Figure 8. - Fan bypass airflow characteristics at engine inlet Reynolds number index of 0.5, no inlet flow distortion.

rotor. The fan bypass airflow ratio is given in figure 8.

Fan performance. - The performance of the outer (tip) annulus of the fan (fig. 4) is presented as the pressure ratio $P_{t,2.6f}/P_{t,2}$ (fan duct total pressure to inlet total pressure) as a function of the corrected total airflow $W_{a,t}\sqrt{\theta_2}/\delta_2$ and corrected fan speed $N_1/\sqrt{\theta_2}$. The symbols are defined in appendix A. The performance of the inner (hub) annulus (fig. 5) is defined by the pressure ratio $P_{t,2.3}/P_{t,2}$ (fourth-stage inlet to engine inlet total pressure) as a function of the corrected total airflow and fan speed.

For both annuli of the fan, increasing the exhaust nozzle area at a given corrected fan rotor speed resulted in an increase in the corrected total fan flow and a decrease in total-pressure ratio. This total-pressure ratio decrease is greater for the outer annular section than for the inner annulus. These data are in reasonably good agreement with those presented in reference 1. The stall limit lines are the results of stall propagating forward from stalls originating in the high-pressure compressor and low-pressure compressor. These stall limits are in good agreement (±1.0 percent) with those predicted from manufacturer's rig-test data.

Core performance. - The performance maps of the core compressors are presented in figures 6 and 7. The low-pressure compressor data are presented as the total-pressure ratio $P_{t,3}/P_{t,2.3}$ (ninth-stage exit to fourth-stage inlet) as a function of the corrected core airflow $W_{a,c}\sqrt{\theta_{2.3}}/\delta_{2.3}$ (fig. 6(a)) and the rotor speed corrected to conditions at station 2.3 (fig. 6(a)). Figure 7 shows the performance of the high-pressure compressor in the form of the total-pressure ratio $P_{t,4}/P_{t,3}$ as a function of corrected airflow $W_{a,c}\sqrt{\theta_3}/\delta_3$ and rotor speed $N_2/\sqrt{\theta_3}$.

For the low-pressure compressor, the constant exhaust nozzle area operating lines shifted in the direction of reduced pressure ratio as the exhaust nozzle area was reduced. Closing the exhaust nozzle decreases the pressure drop across the low-pressure turbine.

This results in less work being done in the low-pressure compressor (i. e., a smaller pressure rise and an increase in core airflow). These data are again in good agreement with reference 1.

The low-pressure compressor stall data are presented as a plot of total-pressure ratio against corrected rotor speed (fig. 6(b)) instead of against airflow. This is done because the limited amount of transient instrumentation at station 2. 3 resulted in transient airflow measurements which are unreliable. Only the rated nozzle area operating line is shown, to avoid complication. The stall points for this compressor at large exhaust nozzle areas and high rotor speeds were obtained with slow accelerations. Stall points for the lower rotor speeds were obtained by tracing the stall progression forward from high-pressure compressor stalls initiated by fuel steps and slow accelerations. The stall limits are more accurately defined than in reference 1, as a result of improved instrumentation and data analysis techniques.

For the high-pressure compressor (fig. 7), the lines of constant exhaust area shifted toward increased pressure ratio as the exhaust nozzle was decreased. Sixteenth-stage inflow bleed was used to extend the corrected speed lines and define the stall limit curve shown in the figure. Stall data were also obtained by slow accelerations and by fuel steps. These data are in good agreement with those obtained with 16th-stage inflow bleed. The pressure ratio at stall increases with airflow and tends to level off at about 24. 0 pounds per second (11. 0 kg/sec). It would appear that the stall limit would intersect the rated operating line at a flow of approximately 27. 7 pounds per second (12. 6 kg/sec).

Compressor stall margins. - The stall margin used in this report considers only the difference in total-pressure ratio at stall and at the operating line for a constant corrected rotor speed. The stall margin in percent is then defined as $100\left[PR_s/(PR_o - 1)\right]_N$ where the subscript o refers to the operating line and s to the stall line, N denotes constant rpm, and PR is the total-pressure ratio. Only the rated nozzle area operating line is considered.

Using this definition, the stall margin for the fan varied from 36 percent at a corrected speed of 6000 rpm to 31 percent at 8000 rpm for the tip section, and from 6 percent at 6000 rpm to 13 percent at 8000 rpm for the hub section. The low-pressure compressor stall margin was approximately 7. 5 percent at 5500 rpm and 8 percent at 6500 rpm. The stall margin for the high-pressure compressor varied from 21 percent at a corrected rotor speed of 9200 rpm to 13 percent at 10 200 rpm.

Bypass ratio. - Figure 8 shows the fan bypass ratio $W_{a,f}/W_{a,c}$ as a function of exhaust area and fan speed. The bypass ratio increased as the exhaust nozzle area was increased at a given corrected fan speed and as corrected fan speed was reduced at a given exhaust nozzle area. As the bypass ratio increased, the fraction of total airflow increased through the fan duct and decreased through the core. These data show a slight increase in the fan bypass ratio compared to that reported in reference 1. This

difference is primarily attributed to an improvement in the measurement of core airflow.

Stage-Group Characteristics

The performance of a compressor stage or stage group is uniquely expressed in terms of nondimensional pressure ψ and flow φ coefficients (ψ and φ are defined in appendix B). Together these form the stage (or stage-group) characteristic. The value of this approach lies in the fact that the pressure coefficient is near peak values at stall, regardless of operating conditions such as rotor speed and inlet pressure (ref. 7). The fan and compressor units have been divided into stage groups and instrumented as shown in figure 1. Stage-group characteristics have been computed for uniform inlet flow and steady-state engine operation (figs. 9 to 14). The flow coefficients for the low- and high-pressure compressor stage groups are based on values at the inlet of each stage group. Because of the complex flow field between the fan hub and tip sections, the flow coefficient for these regions is an average of the fan inlet flow coefficient and each sector's exit flow coefficient (2 to 2.3f and 2 to 2.3).

Fan characteristics. - Figure 9 shows that the fan characteristic for the outer an-

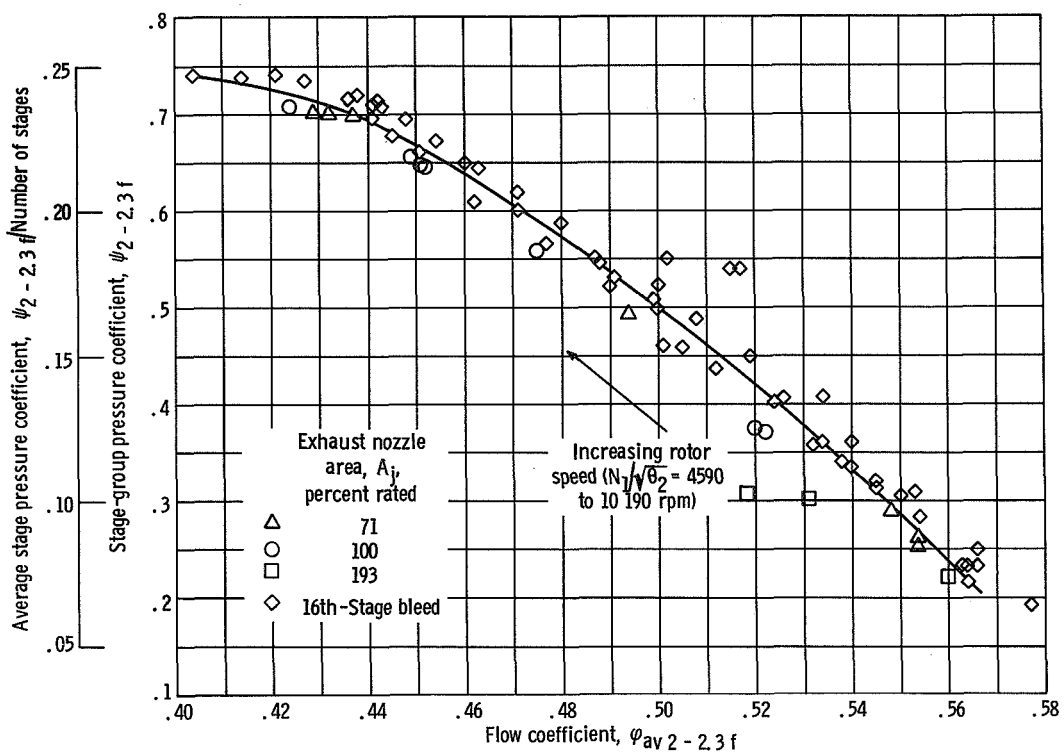

Figure 9. - Fan outer annulus stage-group characteristic (stages 1 to 3).

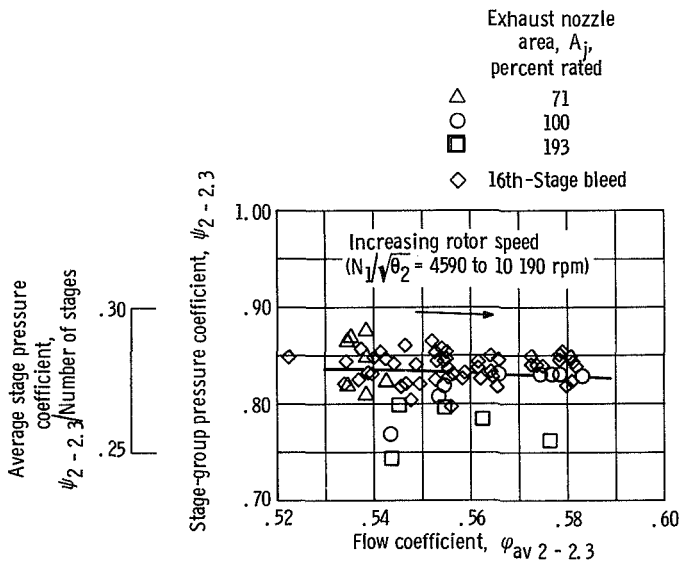

Figure 10. - Fan inner annulus stage-group characteristic (stages 1 to 3).

nulus (2 to 2.3 f) has broad ranges in values for pressure and flow coefficients, indicating a large operating range. With increasing rotor speed, the pressure coefficient of the tip section increases towards stall, and the stall margin decreases. For the hub section, data of figure 10 show practically no variation in the pressure coefficient and only a small increase in the flow coefficient with speed. The hub section would probably have less stall margin than the tip section because the pressure coefficient for the inner annulus varies little from its peak value (0.75 to 0.87), while the outer annulus pressure coefficient has large latitude (0.20 to 0.74). These observations are consistent with previous discussion in the section Compressor stall margins.

Low-pressure compressor. - Figures 11 and 12 show the characteristics for the inlet and exit stage groups of the low-pressure compressor. The inlet stage-group characteristic has the shape and speed variation of a typical compressor inlet stage (refs. 7 to 9) in that the pressure coefficient decreases as the rotor speed is increased. The inlet stage-group characteristic is also affected by engine exhaust nozzle area. The characteristic curve is lowered as the exhaust nozzle area is decreased.

The exit stage group is very flat and is primarily influenced by the engine exhaust nozzle area. Figure 12 shows that the exit stage-group flow coefficient increases as the exhaust nozzle area is decreased. This agrees with a decrease in pressure rise and an increase in airflow with smaller nozzle areas, as stated previously. Since this characteristic is flatter than the usual, the low-pressure compressor is expected to have a lower stall margin because it operates near peak loading. The low-preassure compressor exit stage group has a higher pressure coefficient (1.20 to 1.40) than the inlet stage group (0.85 to 1.12) and both are higher than the fan stage groups.

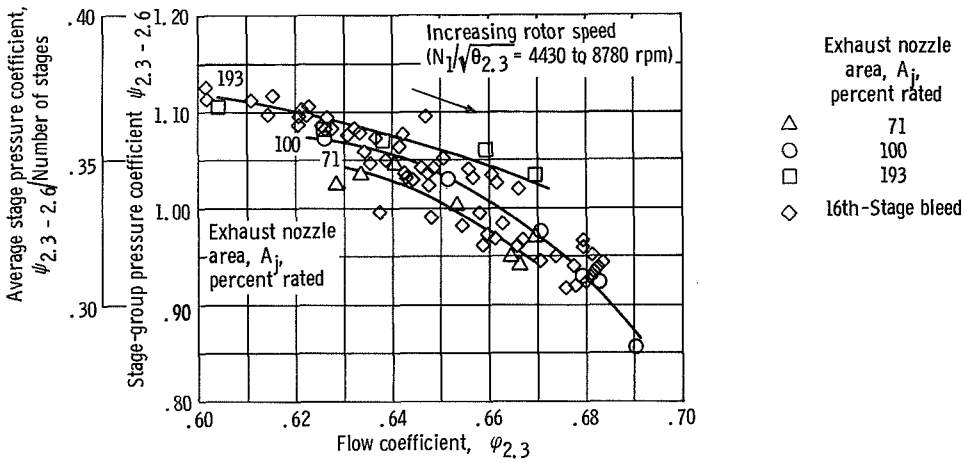

Figure 11. - Low-pressure compressor inlet stage-group characteristic (stages 4 to 6).

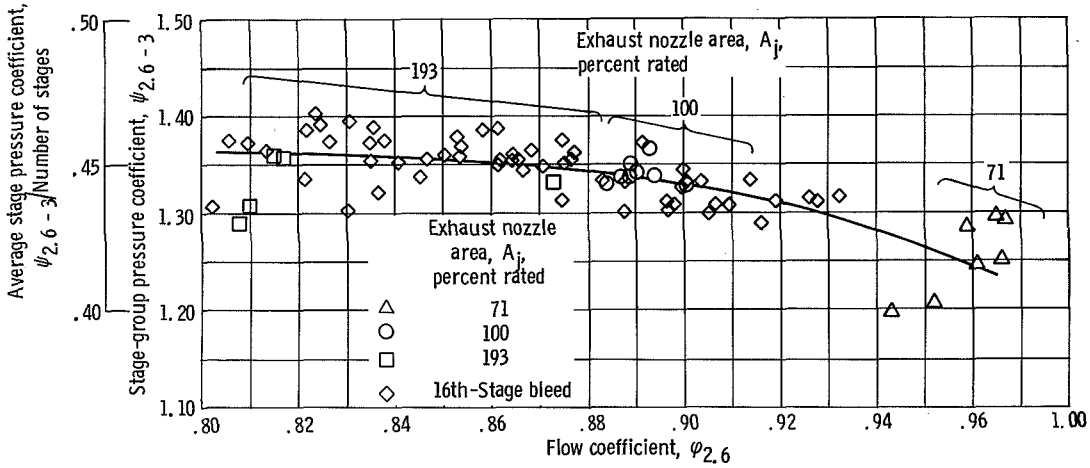

Figure 12. - Low-pressure compressor outlet stage-group characteristic (stages 7 to 9).

High-pressure compressor. - Figure 13 presents the inlet stage-group characteristic and figure 14 the exit stage-group characteristic for the high-pressure compressor. The pressure coefficient ψ decreases for the inlet stage group and increases for the exit stage group with increases in rotor speed. The stall margin then increases in the inlet stage group and decreases in the outlet group with increasing speed. In addition to changes with rotor speed, the pressure coefficient for the inlet stage group tends to decrease as the exhaust nozzle area is increased. The shape of the curve for the last four stages (13 to 16) is similar to the compressor exit characteristics of references 7 and 9 and indicates operation from near choked flow to near stall as speed is increased. The outlet group of four stages operates over a greater load range (ψ = 0.60 to 1.04) than does the inlet group of three stages (ψ = 0.87 to 1.01) and the loading of each stage group is lower than for the exit stage group of the low-pressure compressor.

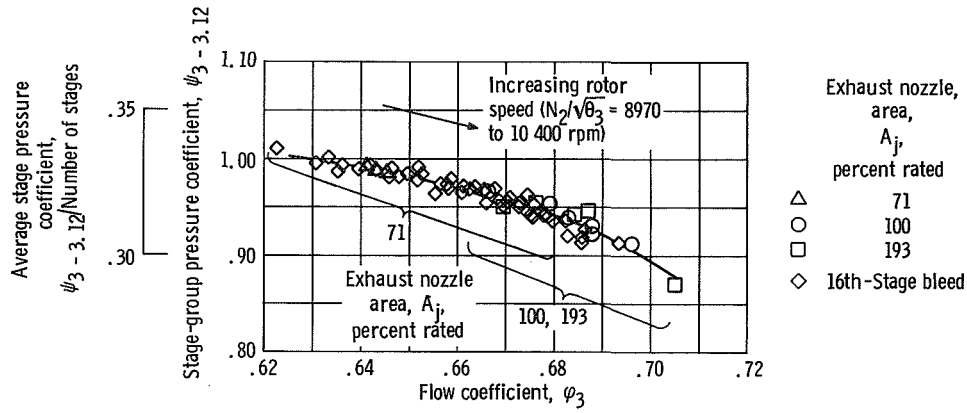

Figure 13. - High-pressure compressor inlet stage-group characteristic (stages 10 to 12).

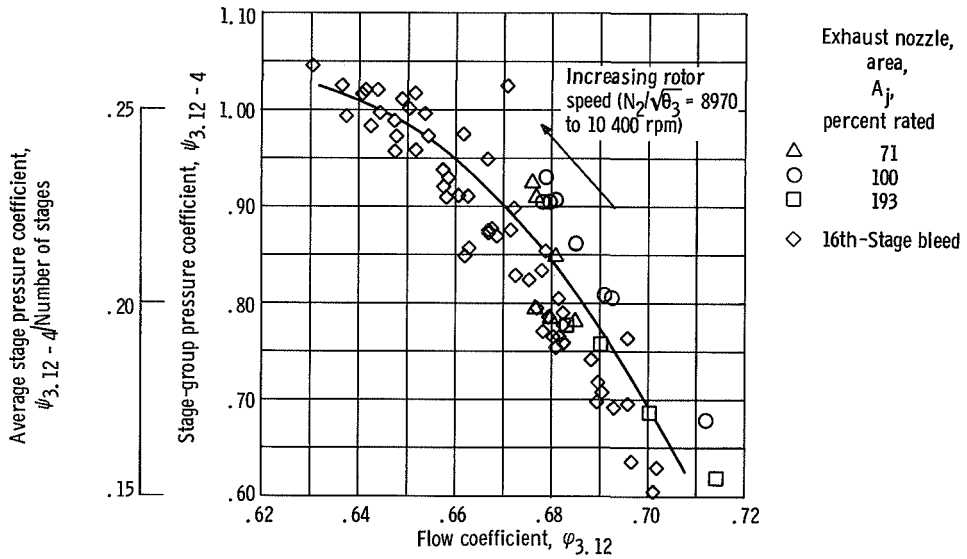

Figure 14. - High-pressure compressor outlet stage-group characteristic (stages 13 to 16).

Effect of 180° Circumferential Distortion

Engine inlet flow distortion pattern. - Figure 15 shows the inlet total-pressure, static-pressure, and Mach number profiles for two screen solidities at about the same airflow. The total pressures are averaged for each of the eight inlet rakes. The static-pressure profile results from the engine trying to induce a constant inlet velocity profile (refs. 3 and 4). The increase in Mach number at the edge of the screen is the apparent result of flow to the low-pressure area behind the screen. The rakes, however, were on a 45° spacing, and a much closer spacing would be required to adequately define this trend.

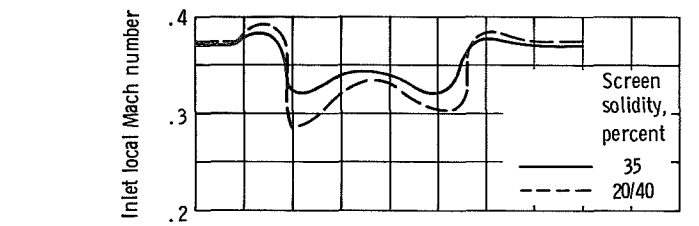

(a) Mach number.

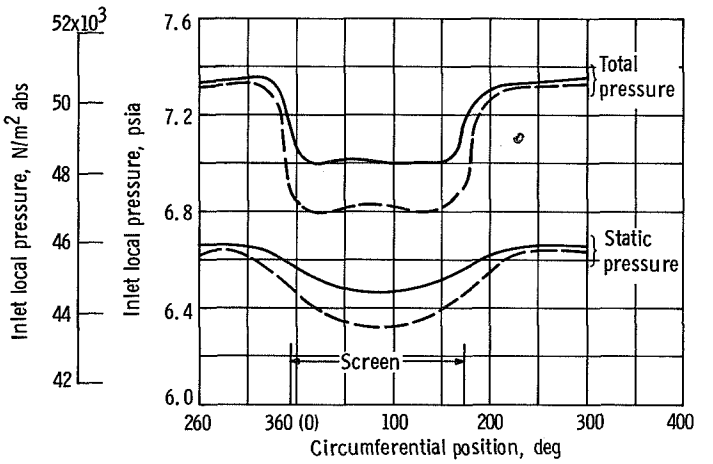

(b) Pressure.

Figure 15. - Compressor inlet profiles with 180° distortion at corrected airflow of 176 pounds per second (80 kg/sec).

The contour map (fig. 16(a)) shows the local total-pressure variation (in percent) from the average total pressure for the same 20/40 percent solidity screen distortion data shown in figure 15. The relative steepness of the pressure gradient at 0° may be due in part to the edge of the screen being 6° on the high-pressure side of the 0° rake, possibly resulting in an improper fairing of the profiles. For purposes of comparison, figure 16(b) presents a uniform inlet flow contour at, however, a higher corrected airflow.

Pressure distortion parameter. - The pressure distortion parameter K_{D2} (see appendix B) is shown in figure 17(a) as a function of screen solidity and corrected airflow. For each of the indicated screen solidities, the airflow was increased, increasing the distortion, until the engine stalled. The observed stall limit for the different levels of distortion is shown along with an estimate of the distortion limit of the engine. This estimate was based on the manufacturer's sea-level rig-test data adjusted for Reynolds number index as well as for any particular features of this engine. The agreement between the estimated and experimental limit is considered to be good.

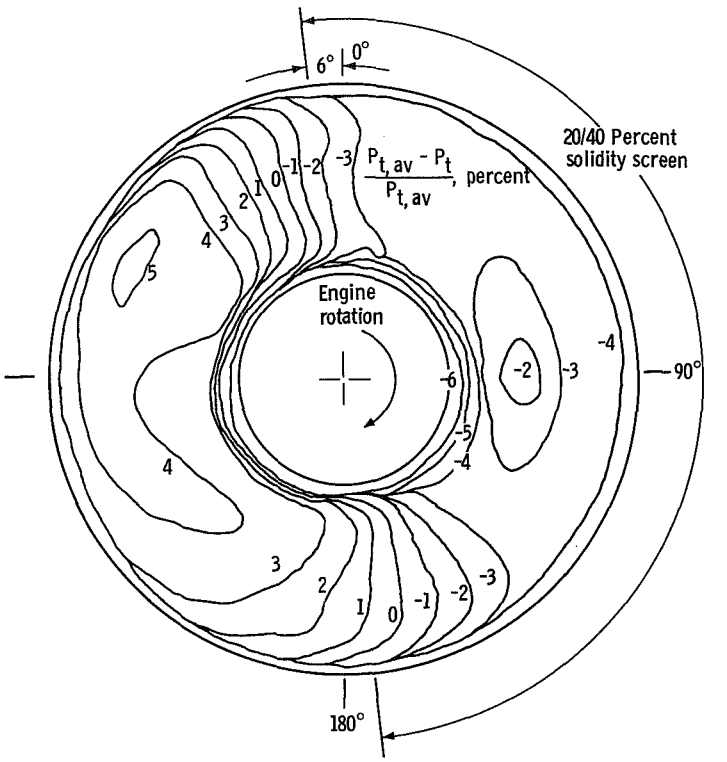

(a) Inlet distortion of 180° at corrected airflow of 176 pounds per second (80 kg/sec).

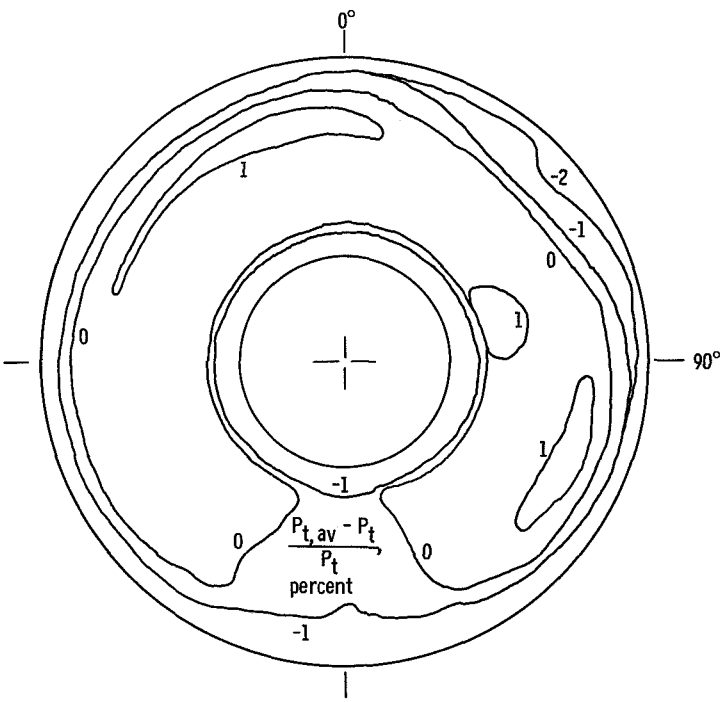

(b) Uniform inlet flow at corrected airflow of 239 pounds per second (108.5 kg/sec).

Figure 16. - Inlet total-pressure contour, looking upstream.

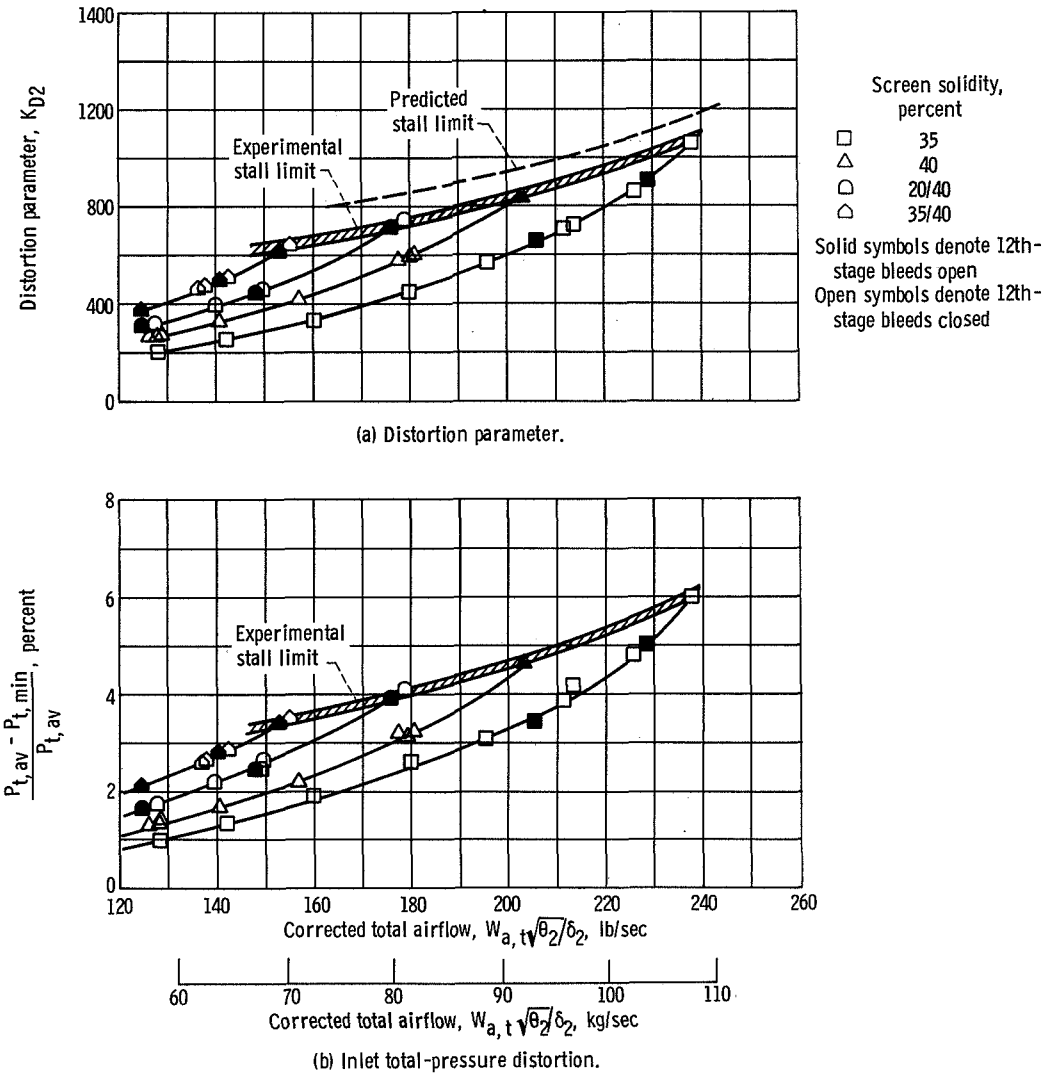

Figure 17. - Engine stall limits resulting from 180° screen distortion at Reynolds number index of 0.5 and at rated exhaust nozzle area.

Also shown in figure 17 is the level of flow distortion in terms of average and minimum total pressure. The data presented are for the fourth radial position from the outer duct wall at station 2 (see fig. 1).

Distortion measurements at stall conditions were taken with the 12th-stage bleeds open, as described in the section Operational Procedure. For any given screen, both the bleeds-open and bleeds-closed data fall along the same line, establishing the validity of this approach.

Effect on performance. - The effects of 180° distortion on performance and stall limits of the fan and compressor for operation with rated exhaust nozzle area are presented in figures 18 to 21.

The influence of various levels of inlet flow distortion on the outer and inner annuli

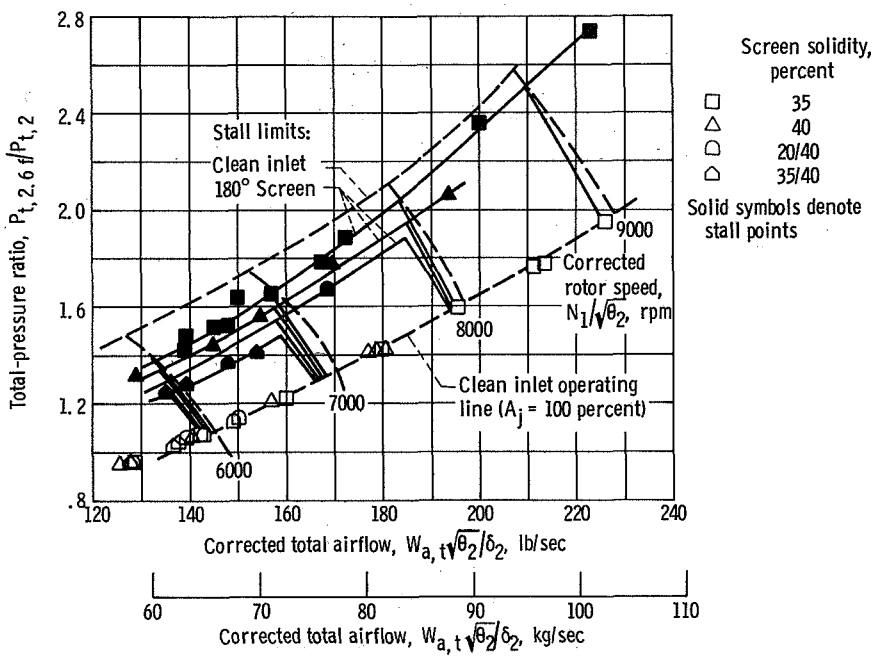

Figure 18. - Effect of 180° distortion on fan outer annulus performance at engine inlet Reynolds number index of 0.5 and at rated exhaust nozzle area.

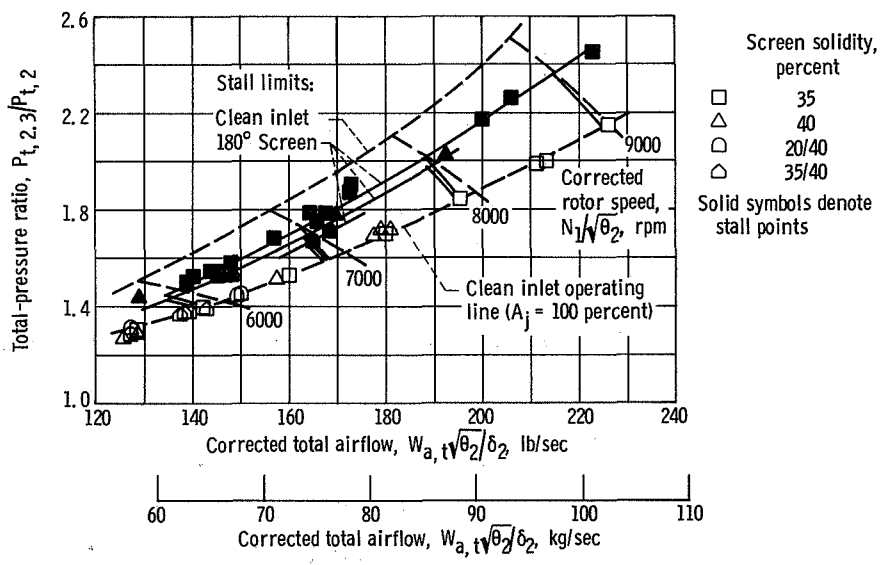

Figure 19. - Effect of 180° distortion on fan inner annulus performance for engine inlet at Reynolds number index of 0.5 and at rated exhaust nozzle area.

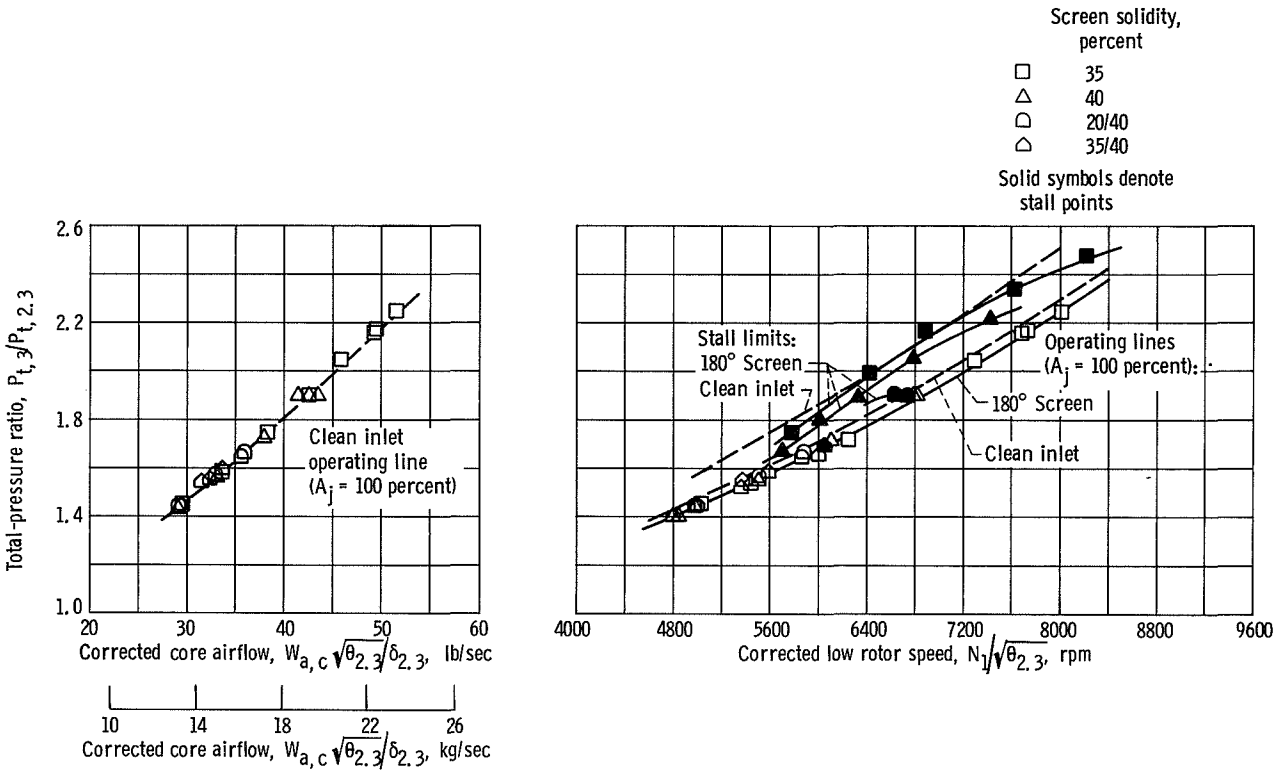

(a) Steady-state performance.

(b) Stall performance.

Figure 20. - Effect of 180° distortion on low-pressure compressor performance at engine inlet Reynolds number index of 0.5 and at rated exhaust nozzle area.

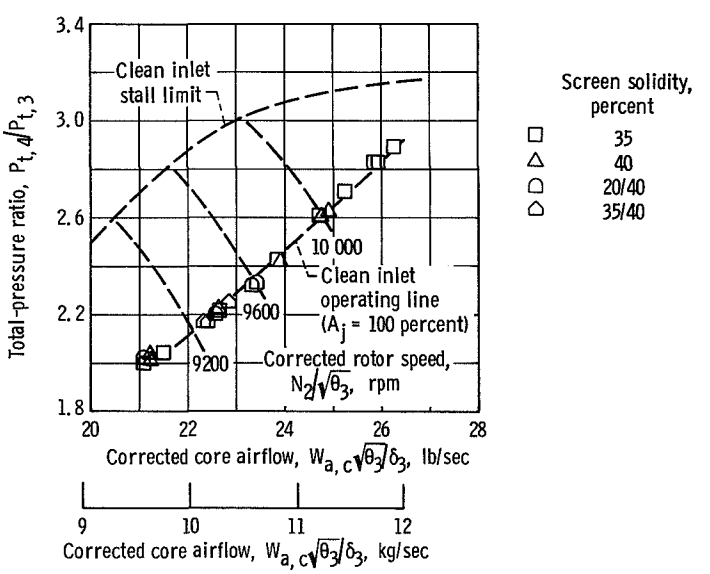

Figure 21. - Effect of 180° distortion on high-pressure compressor performance at engine inlet Reynolds number index of 0.5 and at rated exhaust nozzle area.

of the fan is shown in figures 18 and 19. For both maps, the rated nozzle area operating line remained unchanged except for a slight decrease in performance at constant speed. The stall lines are lowered with increasing levels of inlet flow distortion.

Figure 20(a) shows that the rated nozzle area operating line for the low-pressure compressor remains unchanged with all levels of distortion studied. A loss in performance at constant rotor speed occurred, however, as indicated in figure 20(b). Inlet flow distortion caused the stall line to be lowered sufficiently to intersect the operating line. As the distortion level is increased, the stall line intersects the operating line at progressively lower values of pressure ratio and corrected rotor speed.

The high-pressure compressor performance (fig. 21) apparently is unaffected by the inlet flow distortions, as the pressure distortion is attenuated by the time it enters this compressor. Temperature distortions which usually result as the pressure distortion is attenuated were not detected at the high-pressure compressor inlet. Stall was not observed in the high-pressure compressor when operating with fan inlet distortion, and therefore the effect on the stall limit was not determined.

Stage-group characteristics. - Figures 22 to 27 indicate the effect of a 35 percent solidity screen distortion on the overall stage-group characteristics under steady-state engine operation. The tip section of the fan (fig. 22) shows a decrease in pressure and flow coefficients from the uniform flow characteristic. This shift means a decrease in work and flow with inlet flow distortion. The hub section pressure coefficient (fig. 23) decreases slightly and is relatively constant with changes in the flow coefficient.

The low-pressure compressor inlet and outlet stage groups (figs. 24 and 25) show a decrease in pressure and flow coefficients with inlet flow distortion. As indicated by figure 24, the inlet stage-group characteristic for the different nozzle areas can be represented by a single curve. The curves for the fan hub and the low-pressure compressor stage groups became slightly flatter with distortion; this could indicate a decrease in the overall stall margin for each stage group.

The high-pressure compressor (figs. 26 and 27) has little shift in its characteristics as the inlet flow was distorted. This suggests that the pressure distortion was attenuated before reaching this unit.

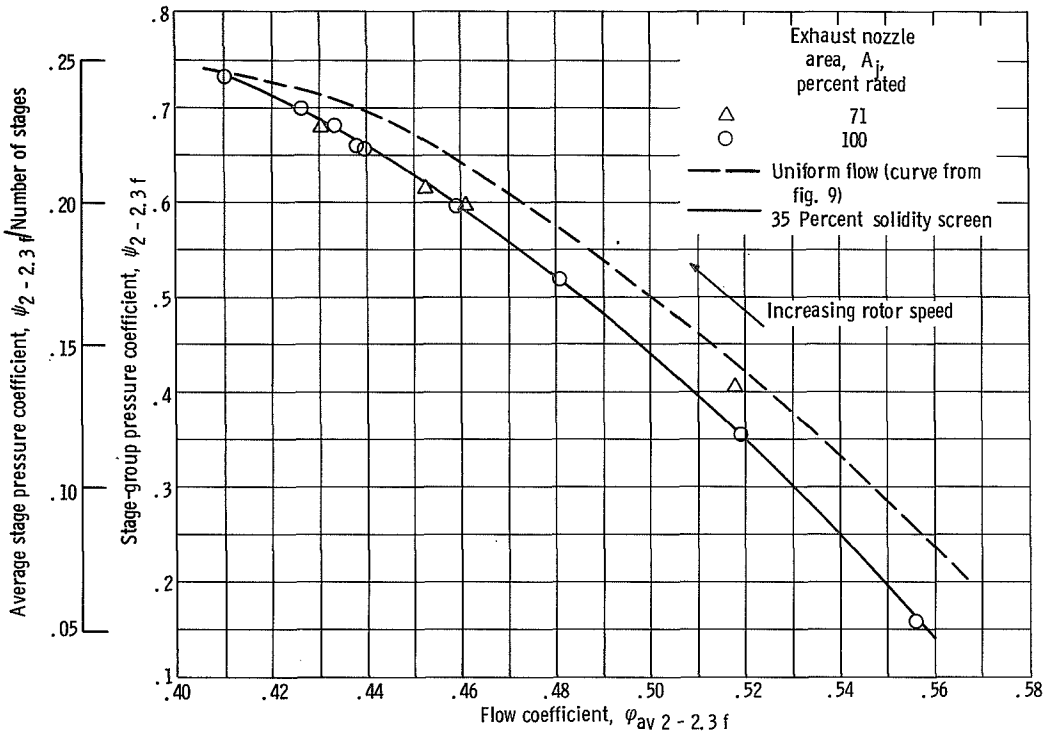

Figure 22. - Effect of 180° distortion on fan outer annulus stage-group characteristic (stages 1 to 3).

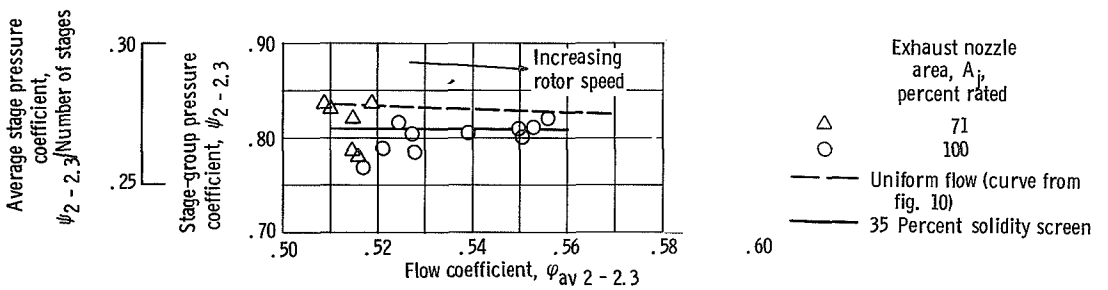

Figure 23. - Effect of 180° distortion on fan inner annulus stage-group characteristic (stages 1 to 3).

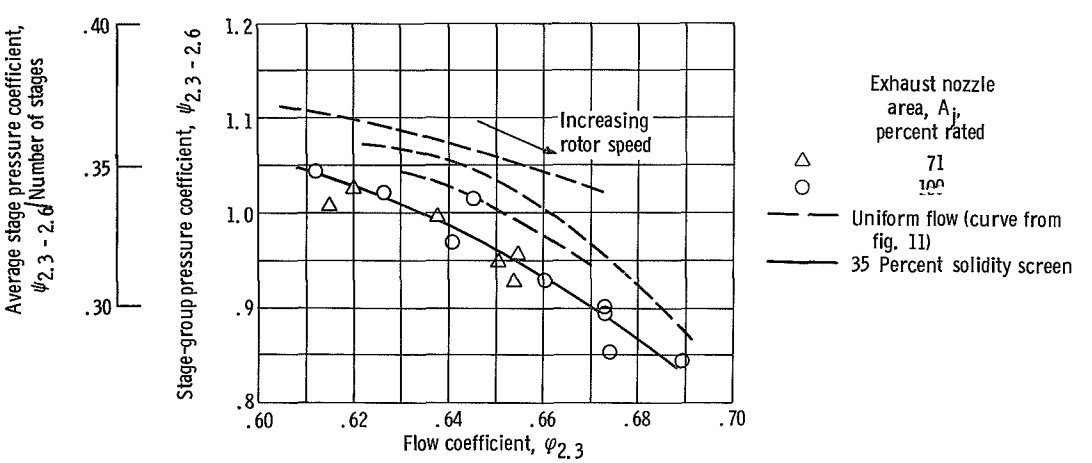

Figure 24. - Effect of 180° distortion on low-pressure compressor inlet stage-group characteristic (stages 4 to 6).

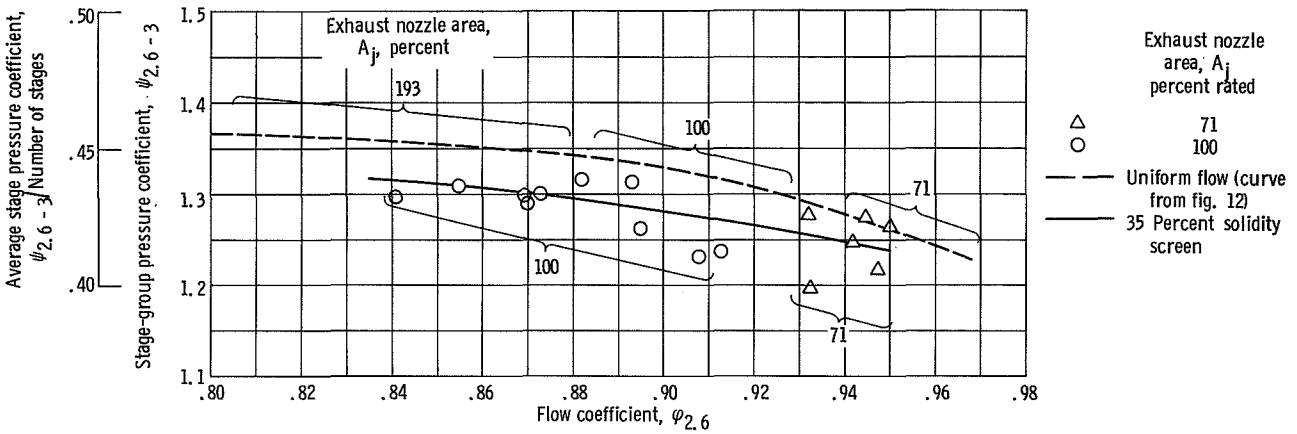

Figure 25. - Effect of 180° distortion on low-pressure compressor outlet stage group characteristic (stages 7 to 9).

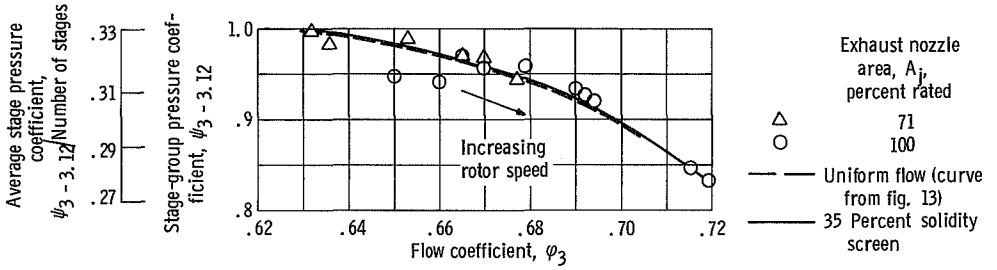

Figure 26. - Effect of 180° distortion on high-pressure compressor inlet stage-group characteristic (stages 10 to 12).

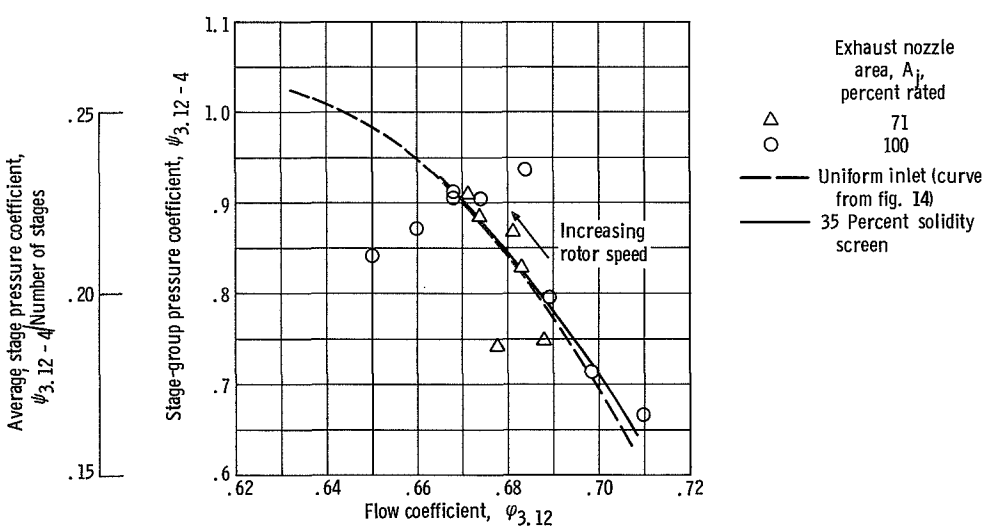

Figure 27. - Effect of 180° distortion on high-pressure compressor outlet stage-group characteristic (stages 13 to 16).

SUMMARY OF RESULTS

An investigation was conducted with a two-spool, afterburner-equipped turbofan engine to obtain a better understanding of the effect of inlet flow field anomalies on engine stability. Presented herein are the results of operation with uniform inlet flow and with inlet flow distortion (screens over an 180^{o} sector of the compressor face).

Uniform Inlet Flow

The following results were obtained with uniform inlet flow:

1. An exhaust nozzle area increase resulted in lowering the fan tip section (outer annulus) operating line more than that for the fan hub section (inner annulus). This area increase raised the low-pressure compressor operating line and lowered the high-pressure compressor operating line.

2. The stall margins (based on pressure ratio difference for a given corrected rotor speed at rated exhaust nozzle area) varied from 36 to 31 percent for the fan tip section, 6 to 13 percent for the fan hub section, 7.5 to 8 percent for the low-pressure compressor, and 21 to 13 percent for the high-pressure compressor, as the speed was increased.

Distorted Inlet Flow

The results obtained with distorted inlet flow are as follows:

1. The maximum value of the inlet distortion parameter K_{D2}, which resulted in stall at 0.5 Reynolds number index, is approximately 1100 (6 percent $\Delta P_t/P_{t,\,av}$) at an inlet corrected airflow of 240 pounds per second (109 kg/sec).

2. For a constant corrected speed, corrected airflow and pressure ratio are reduced in the fan and low-pressure compressor as the inlet flow is distorted.

3. The stall limit lines of the fan tip, fan hub, and low-pressure compressor are lowered as the distortion is increased. The stall lines of the low-pressure compressor intersect the operating line at progressively lower pressure ratios and rotor speeds with increasing distortion.

4. Distortion within the range investigated appears to have little effect on the high-pressure compressor, as evidenced by the fact that the stage group characteristics were

unaffected by inlet flow distortion. The fan and low-pressure compressor characteristics, however, are shifted to lower values of pressure and flow coefficients with inlet flow distortion.

Lewis Research Center,
National Aeronautics and Space Administration,
Cleveland, Ohio, November 7, 1969,
720-03.

APPENDIX A

SYMBOLS

A	flow area, $ft^2(cm^2)$
C	constant
D	diameter, in. (cm)
g	acceleration due to gravity, 32.174 ft/sec^2 (980.66 cm/sec^2)
H	enthalpy, Btu/lb (J/kg)
J	mechanical equivalent of heat, 778 ft-lb/Btu
K_{D2}	Pratt & Whitney distortion factor (see appendix B)
N_1	low-rotor speed, rpm
N_2	high-rotor speed, rpm
P	static pressure, psi (N/cm^2)
PR	pressure ratio
P_t	total pressure, psi (N/cm^2)
R	gas constant, 53.3 ft-lb/lb-^oR (286 J/kg-K)
RNI	Reynolds number index, $\left[\delta/(\mu/\mu_{sl})\sqrt{\theta}\right]$
T	total temperature, ^oR (K)
W_a	airflow rate (weight flow), lb/sec (kg/sec)
Δ	difference between values
δ	ratio of total pressure to standard sea-level static pressure
Θ	angular measure, deg
θ	ratio of total temperature to standard sea-level static temperature
μ	absolute viscosity, $N\text{-}sec/m^2$
φ	flow coefficient (see appendix B for definitions)
ψ	pressure coefficient (see appendix B for definitions)

Subscripts:

a	absolute
av	average
c	core
f	fan duct
j	exhaust nozzle
o	operating line
r	ring
s	stall line
sl	sea level
t	total condition
1, 7	instrumentation station location

APPENDIX B

DEFINITIONS

Pratt & Whitney Distortion Factor, K_{D2}

The distortion parameter K_{D2} is defined by the following equation:

$$K_{D2} = \frac{\sum_{r=1}^{n} \bar{\Theta}_r \left(\frac{\Delta P_t}{P_t}\right)_r \frac{OD}{D_r}}{\sum_{r=1}^{n} \frac{OD}{D_r}}$$

The terms appearing in the equation for K_{D2} are defined as follows:

r — a particular ring of total-pressure probes

$\bar{\Theta}_r$ — circumferential extent of largest single pressure depression below $P_{t,\,av}$, in degrees, for a particular ring (see following sketch)

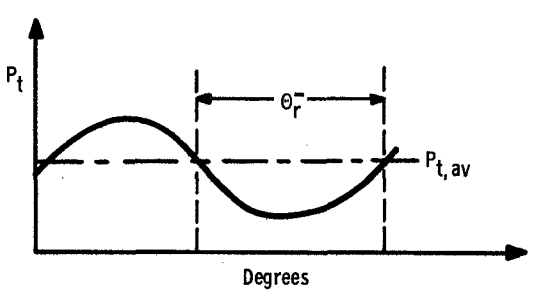

$\left(\frac{\Delta P_t}{P_t}\right)_r$ — $\frac{P_{t,\,av} - P_{t,\,min}}{P_{t,\,av}}$, in percent, for a particular ring

$P_{t,\,av}$ — average pressure per ring

$P_{t,\,min}$ — minimum pressure per ring

OD — outside diameter of duct

D_r diameter of a particular ring

n number of measurement rings

Compressor Parameters

Flow coefficient. - The flow coefficient is defined by the following equation:

$$\varphi = C_{\varphi} \frac{W_a \frac{\sqrt{\theta}}{\delta}}{\frac{N}{\sqrt{\theta}}}$$

The term C_{φ} is defined as $\left[(60)(R)(519)\right] / \left[(\pi)(D)(A)(14.69)\right]$, where D is the mean diameter.

Pressure coefficient. - The pressure coefficient is defined by the following equation:

$$\psi = C_{\psi} \frac{\Delta H_{isentropic}}{\left(\frac{N}{\sqrt{\theta}}\right)^2}$$

The term C_{ψ} is defined as $(g)(J)(60/\pi D)^2$, where D is the mean diameter.

APPENDIX C

HIGH-RESPONSE INSTRUMENTATION

Probe Design

Due to the nature of the research program, it was necessary to utilize high-response instrumentation that had the capability of reliably measuring pressure variations of 300 hertz with a maximum amplitude error of ±5 percent. To meet this requirement, minature $\frac{1}{4}$-inch-diameter pressure transducers, small enough to be mounted in the pressure-rake body itself, were used, as discussed in reference 1.

This feature makes it possible for the transducers to be short-coupled (1 to 2 in.) to their sensing points in the gas stream. Because the transducers were limited to a 170° F (76.5° C) operating temperature and had significant calibration shifts with tem-

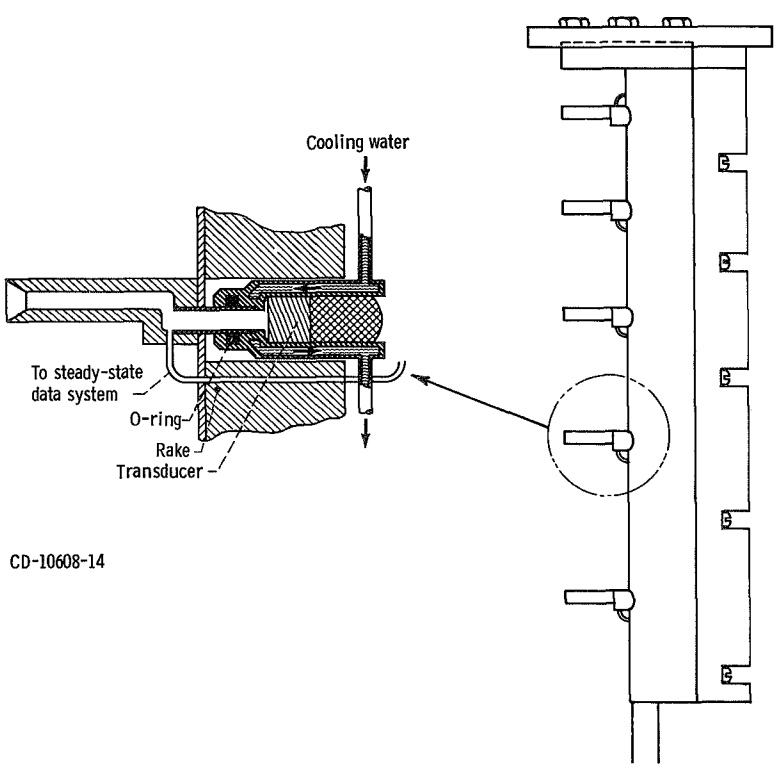

(a) Compressor inlet rake.

Figure 28. - Typical probe installation.

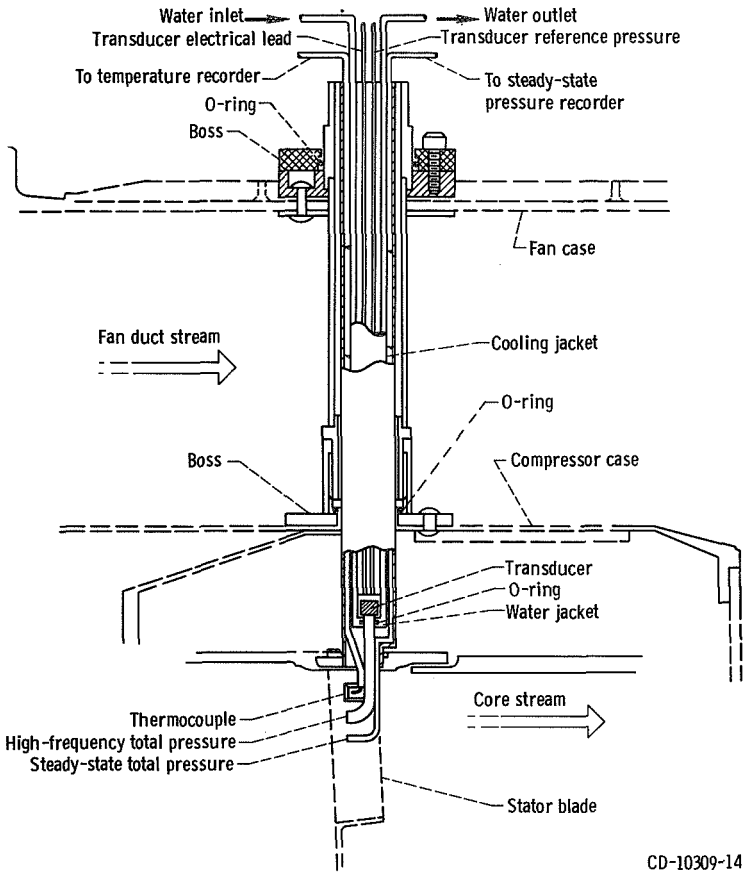

(b) Interstage probe.

Figure 28. - Concluded.

perature changes, water cooling was employed. The transducers, mounted in the water jackets, could be removed for repair without removing the complete rake from the engine. Typical probe installations are shown in figure 28.

Due to the design requirements of the probes, some of the coupling lengths were longer than desired. The following table shows the coupling lengths and frequency response of the probes for various instrumentation locations throughout the engine:

Station	Coupling length		Response, Hz
	in.	cm	
2	1.45	3.68	375
2.3 f	2.25	5.71	220
2.3	2.20	5.59	230
2.6	2.25	5.71	220
3	1.60	4.06	350
3.12	1.35	3.43	415
4	2.50	6.35	190

Calibration System

Preliminary calibration of these miniature transducers indicated that zero and sensitivity shifts occurred as a function of time and were not predictable. Thus, the prerun calibrations could not be relied on for any extended period of time. Therefore, a system was devised to calibrate these transducers in their operating environment inside the engine just prior to recording transient data. These transducers were only used to measure the pressure change from the steady-state values existing just prior to the transient. A schematic of the calibration system is shown in figure 29.

The calibration of these miniature ΔP transducers consisted of observing the change in output for two values of reference pressure. The engine pressures were held constant by maintaining steady-state conditions. One reference pressure was a constant of approximately 5 psia (3.4 N/cm^2 abs). The second reference pressure was obtained from the engine by using the normal steady-state pressure probes. The transducer reference pressure lines were connected to reference mainfolds. There were four such manifolds, each using a different engine pressure level as a reference. Three-way valves were utilized to connect first the constant 5-psia (3.4 N/cm^2 abs) pressure and then the engine pressures to the reference manifolds to establish the calibration sequence. The sensitivity of the transducers is the ratio of the change in reference pressure to the change in transducer output. The second, or engine reference pressure, was maintained constant during the transient. The base pressure levels for these transient measurements were obtained from an adjacent steady-state pressure measurement.

The high-frequency response data were recorded simultaneously on a high-speed digitizer-recorder and on magnetic tape. The digital recorder had a sampling rate of approximately 50 samples per second per channel. Therefore, these data were used only to follow the transient up to the point of stall. The actual stall point and time sequence were obtained from the analog traces made from the magnetic tape.

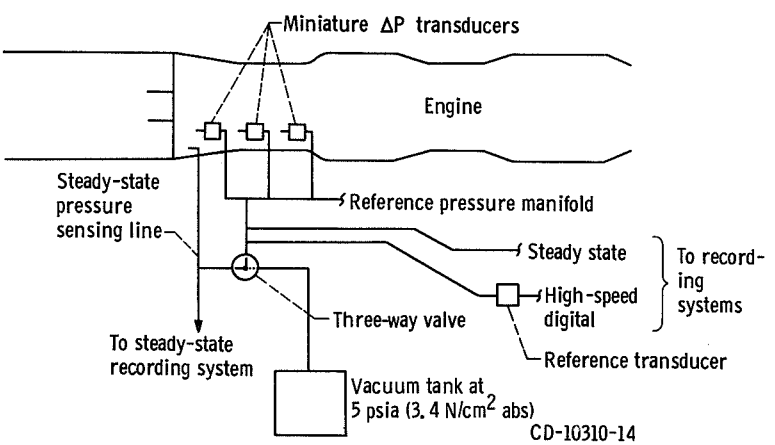

Figure 29. - Reference system used for transient instrumentation calibration.

REFERENCES

1. Braithwaite, Willis M.; and Vollmar, William R.: Performance and Stall Limits of a YTF30-P-1 Turbofan Engine with Uniform Inlet Flow. NASA TM X-1803, 1969.

2. Huntley, S. C.; Sivo, Joseph N.; and Walker, Curtis L.: Effect of Circumferential Total-Pressure Gradients Typical of Single-Inlet Duct Installations on Performance of an Axial-Flow Turbojet Engine. NACA RM E54K26a, 1955.

3. Langston, C. E.: Distortion Tolerance - by Design Instead of by Accident. Paper 69-GT-115, ASME, Mar. 1969.

4. Reid, C.: The Response of Axial Flow Compressor to Intake Flow Distortion. Paper 69-GT-29, ASME, Mar. 1969.

5. Smith, Ivan D.; Braithwaite, W. M.; and Calvert, Howard F.: Effect of Inlet-Air-Flow Distortions on Steady-State Performance of J65-B-3 Turbojet Engine. NACA RM E55I09, 1956.

6. Staff of Lewis Laboratory: Central Automatic Data Processing System. NACA TN 4212, 1958.

7. Lubick, Robert J.; and Wallner, Lewis E.: Stall Prediction in Gas-Turbine Engines. J. Basic Eng., vol. 81, no. 3, Sept. 1959, pp. 401-408.

8. Calvert, Howard F.; Braithwaite, Willis M.; and Medeiros, Arthur A.: Rotating-Stall and Rotor-Blade-Vibration Survey of a 13-Stage Axial-Flow Compressor in a Turbojet Engine. NACA RM E54J18, 1955.

9. Harry, David P., III; and Lubick, Robert J.: Inlet-Air Distortion Effects on Stall, Surge, and Acceleration Margin of a Turbojet Engine Equipped with Variable Compressor Inlet Guide Vanes. NACA RM E54K26, 1955.

10. Mechtly, E. A.: The International System of Units, Physical Constants and Conversion Factors. NASA SP-7012, 1964.

NASA-Langley, 1970 —— 28 E-5352

NATIONAL AERONAUTICS AND SPACE ADMINISTRATION
WASHINGTON, D.C. 20546

OFFICIAL BUSINESS

FIRST CLASS MAIL

POSTAGE AND FEES PAID
NATIONAL AERONAUTICS AN
SPACE ADMINISTRATION

POSTMASTER: If Undeliverable (Section 158
Postal Manual) Do Not Return

"The aeronautical and space activities of the United States shall be conducted so as to contribute . . . to the expansion of human knowledge of phenomena in the atmosphere and space. The Administration shall provide for the widest practicable and appropriate dissemination of information concerning its activities and the results thereof."

—NATIONAL AERONAUTICS AND SPACE ACT OF 1958

NASA SCIENTIFIC AND TECHNICAL PUBLICATIONS

TECHNICAL REPORTS: Scientific and technical information considered important, complete, and a lasting contribution to existing knowledge.

TECHNICAL NOTES: Information less broad in scope but nevertheless of importance as a contribution to existing knowledge.

TECHNICAL MEMORANDUMS: Information receiving limited distribution because of preliminary data, security classification, or other reasons.

CONTRACTOR REPORTS: Scientific and technical information generated under a NASA contract or grant and considered an important contribution to existing knowledge.

TECHNICAL TRANSLATIONS: Information published in a foreign language considered to merit NASA distribution in English.

SPECIAL PUBLICATIONS: Information derived from or of value to NASA activities. Publications include conference proceedings, monographs, data compilations, handbooks, sourcebooks, and special bibliographies.

TECHNOLOGY UTILIZATION PUBLICATIONS: Information on technology used by NASA that may be of particular interest in commercial and other non-aerospace applications. Publications include Tech Briefs, Technology Utilization Reports and Notes, and Technology Surveys.

Details on the availability of these publications may be obtained from:

SCIENTIFIC AND TECHNICAL INFORMATION DIVISION

NATIONAL AERONAUTICS AND SPACE ADMINISTRATION

Washington, D.C. 20546